

# Improvement of Recovering Shape from Endoscope Images Using RBF Neural Network

Yuji Iwahori<sup>1</sup>, Seiya Tsuda<sup>1</sup>, Robert J. Woodham<sup>2</sup>, M. K. Bhuyan<sup>3</sup> and Kunio Kasugai<sup>4</sup>

<sup>1</sup>*Dept. of Computer Science, Chubu University, Kasugai 487-8501, Japan*

<sup>2</sup>*Dept. of Computer Science, University of British Columbia, Vancouver V6T 1Z4, Canada*

<sup>3</sup>*Dept. of Electronics and Electrical Engineering, Indian Institute of Technology Guwahati, Guwahati 781039, India*

<sup>4</sup>*Dept. of Gastroenterology, Aichi Medical University, Nagakute 480-1195, Japan*

**Keywords:** Endoscope Image, VBW Model, RBF-NN, Shape Modification, Reflection Factor.

**Abstract:** The VBW (Vogel-Breuß-Weickert) model is proposed as a method to recover 3-D shape under point light source illumination and perspective projection. However, the VBW model recovers relative, not absolute, shape. Here, shape modification is introduced to recover the exact shape. Modification is applied to the output of the VBW model. First, a local brightest point is used to estimate the reflectance parameter from two images obtained with movement of the endoscope camera in depth. After the reflectance parameter is estimated, a sphere image is generated and used for Radial Basis Function Neural Network (RBF-NN) learning. The NN implements the shape modification. NN input is the gradient parameters produced by the VBW model for the generated sphere. NN output is the true gradient parameters for the true values of the generated sphere. Depth can then be recovered using the modified gradient parameters. Performance of the proposed approach is confirmed via computer simulation and real experiment.

## 1 INTRODUCTION

Endoscopy allows medical practitioners to observe the interior of hollow organs and other body cavities in a minimally invasive way. Sometimes, diagnosis requires assessment of the 3-D shape of the observed tissue. For example, the pathological condition of a polyp often is related to its geometrical shape. Medicine is an important area of application of computer vision technology. Specialized endoscopes with a laser light beam head (Nakatani et al., 2007) or with two cameras mounted in the head (Mourgues et al., 2001) have been developed. Many approaches are based on stereo vision (Thormaehlen et al., 2001). However, the size of the endoscope becomes large and this imposes a burden on the patient. Here, we consider a general purpose endoscope, of the sort still most widely used in medical practice.

Shape recovery from endoscope images is considered. Shape from shading (SFS) (Horn, 1975) and Fast Marching Method (FMM) (Sethian, 1996) based SFS approach (Kimmel and Sethian, 2001) are proposed. These approaches assume orthographic projection. An extension of FMM to perspective projection is proposed in (Yuen et al., 2007). Further ex-

tension of FMM to both point light source illumination and perspective projection is proposed in (Iwahori et al., 2010). Recent extensions include generating a Lambertian image from the original multiple color images (Ding et al., 2010), (Neog et al., 2011). Application of FMM includes solution (Iwahori et al., 2014) under oblique illumination using neural network learning (Ding et al., 2009). Most of the previous approaches treat the reflectance parameter as a known constant. The problem is that it is impossible to estimate the reflectance parameter from only one image. Further, it is also difficult to apply point light source based photometric stereo (Iwahori et al., 1990) in the context of endoscopy.

Iwahori et al. (Iwahori et al., 1997) developed Radial Basis Function Neural Network (RBF-NN) photometric stereo, exploiting the fact that an RBF-NN is a powerful technique for multi-dimensional non-parametric functional approximation.

Recently, the Vogel-Breuß-Weickert (VBW) model (Vogel et al., 2007), based on solving the Hamilton-Jacobi equation, has been proposed to recover shape from an image taken under the conditions of point light source illumination and perspective

projection. However, the result recovered by the VBW model is relative. VBW gives smaller values for surface gradient and height distribution compared to the true values. That is, it is not possible to apply the VBW model directly to obtain exact shape and size.

This paper proposes a new approach to improve the accuracy of polyp shape determination as absolute size. The proposed approach estimates the reflectance parameter from two images with small camera movement in the depth direction. A Lambertian sphere model is synthesized using the estimated reflectance parameter. The VBW model is applied to the synthesized sphere and shape then is recovered. An RBF-NN is used to improve the accuracy of the recovered shape, where the input to the NN is the surface gradient parameters obtained with the VBW model and the output is the corresponding, corrected true values.

The proposed approach is evaluated via computer simulation and real experiments and it is confirmed that the obtained shape is improved.

## 2 VBW MODEL

The VBW model (Vogel et al., 2007) is proposed as a method to calculate depth (distance from the viewer) under point light source illumination and perspective projection. The method solves the Hamilton-Jacobi equations (Benton, 1977) associated with the models of Faugeras and Prados (Prados and Faugeras, 2004) (Prados and Faugeras, 2003). Lambertian reflectance is assumed.

The following processing is applied to each point of the image. First, the initial value for the depth  $Z_{default}$  is given using Eq.(1) as in (Prados and Faugeras, 2005).

$$Z_{default} = -0.5 \log(I f^2) \quad (1)$$

where  $I$  represents the normalized image intensity and  $f$  is the focal length of the lens.

Next, the combination of gradient parameters which gives the minimum gradient is selected from the difference of depths for neighboring points. The depth,  $Z$ , is calculated from Eq.(2) and the process is repeated until the  $Z$  values converge. Here,  $(x, y)$  are the image coordinates,  $\Delta t$  is the change in time,  $(m, n)$  is the minimum gradient for  $(x, y)$  directions, and  $Q = \frac{f}{\sqrt{x^2 + y^2 + f^2}}$  is the coefficient of the perspective projection.

$$Z(x, y) = Z(x, y) + \Delta t \exp(-2Z(x, y)) - \Delta t \left( \frac{I f^2}{Q} \sqrt{f^2(m(x)^2 + n(y)^2) + (xm(x) + ym(y))^2 + Q^2} \right) \quad (2)$$

Here, it is noted that the shape obtained with the VBW model is given in a relative scale, not an absolute one. The obtained result gives smaller values for surface gradients than the actual gradient values.

## 3 PROPOSED APPROACH

### 3.1 Estimating Reflectance Parameter

When uniform Lambertian reflectance and point light source are assumed, image intensity depends on the dot product of surface normal vector and the light source direction vector subject to the inverse square law for illuminance.

Measured intensity at each surface point is determined by Eq.(3).

$$E = C \frac{(\mathbf{s} \cdot \mathbf{n})}{r^2} \quad (3)$$

where  $E$  is image intensity,  $\mathbf{s}$  is a unit vector towards the point light source,  $\mathbf{n}$  is a unit surface normal vector, and  $r$  is the distance between the light source and surface point.

The proposed approach estimates the value of the reflectance parameter,  $C$ , using two images acquired with a small camera movement in the depth direction. It is assumed that  $C$  is constant for all points on the Lambertian surface. Regarding geometry, it is assumed that both the point light source and the optical center of lens are co-located at the origin of the  $(X, Y, Z)$  world coordinate system. Perspective projection is assumed.

The actual endoscope image has the color textures and specular reflectance. Using the approach proposed by (Shimasaki et al., 2013) the original input endoscope image is converted into one that satisfies the assumptions of a uniform Lambertian gray scale image.

The procedure to estimate  $C$  is as follows.

**Step 1.** If the value of  $C$  is given, depth  $Z$  is uniquely calculated and determined at the point with the local maximum intensity (Tatematsu et al., 2013). At this point, the surface normal vector and the light source direction vector are aligned and produce the local maximum intensity for that value of  $C$ .

**Step 2.** For camera movement,  $\Delta Z$ , in the  $Z$  direction, two images are used and the difference in  $Z$ ,  $Z_{diff}$ , at the local maximum intensity points in each image is calculated. Here the camera movement,  $\Delta Z$ , is assumed to be known.

**Step 3.** Let  $f(C)$  be the error between  $\Delta Z$  and  $Z_{diff}$ .  $f(C)$  represents an objective function to be minimized to estimate the correct value of  $C$ . That is, the value of  $C$  is the one that minimizes  $f(C)$  given in Eq.(4).

$$f(C) = (\Delta Z - Z_{diff}(x,y))^2 \quad (4)$$

### 3.2 NN Learning for Modification of Surface Gradient

The size and shape recovered by the VBW model are relative. VBW gives smaller values for surface gradient and depth compared to the true values. Here, modification of surface gradient and improvement of the recovered shape are considered. First, the surface gradient at each point is modified by a neural network. Then the depth is modified using the estimated reflectance parameter,  $C$ , and the modified surface gradient,  $(p,q) = (\frac{\partial Z}{\partial X}, \frac{\partial Z}{\partial Y})$ . A Radial Basis Function Neural Network (RBF-NN) (Ding et al., 2009) is used to learn the modification of the surface gradient obtained by the VBW model.

Using the estimated  $C$ , a sphere image is synthesized with uniform Lambertian reflectance.

The VBW model is applied to this synthesized sphere. Surface gradients,  $(p,q)$ , are obtained using forward difference of the  $Z$  values obtained from the VBW model.

The estimated gradients,  $(p,q)$ , and the corresponding true gradients for the synthesized sphere,  $(p,q)$ , are given respectively as input vectors and output vectors to the RBF-NN. NN learning is applied.

After NN learning, the RBF-NN can be used to modify the recovered shape for other images.

Two endoscope images, (a) and (b), and the images assuming Lambertian reflectance, (c) and (d), generated using (Shimasaki et al., 2013), are shown

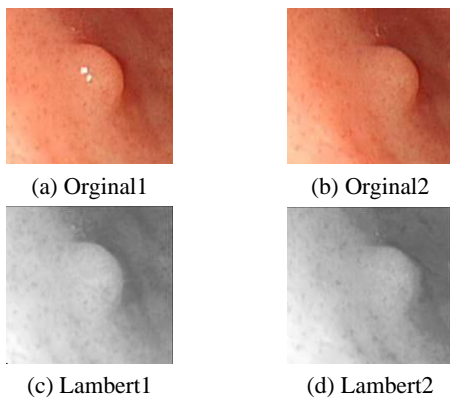


Figure 1: Endoscope Image and Lambertian Image.

in Fig.1.

An example of the objective function,  $f(C)$ , is shown in Fig.2.

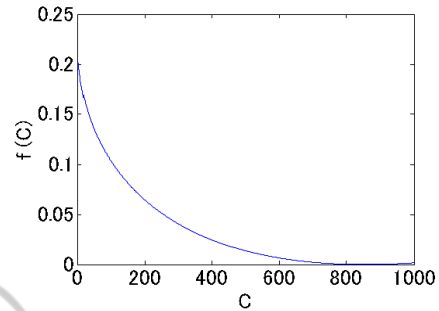
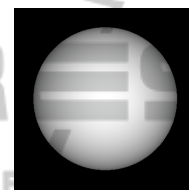
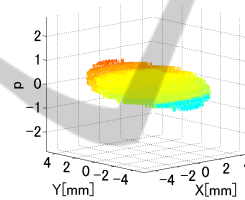


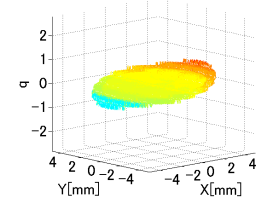
Figure 2: Objective Function  $f(C)$ .



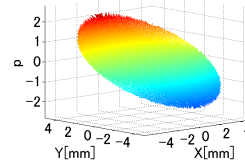
(a) Sphere



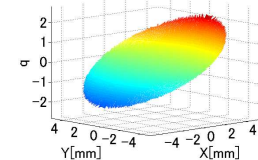
(b)  $p$  by VBW



(c)  $q$  by VBW



(d) True  $p$



(e) True  $q$

Figure 3: Synthesized Sphere for NN Learning.

The synthesized sphere image used in NN learning is shown in Fig.3(a). Surface gradients obtained by the VBW model are shown in Fig.3(b)(c) and the corresponding true gradients for this sphere are shown in Fig.3(d)(e). Points are sampled from the sphere as input for NN learning, except for points with large values of  $(p,q)$ . The procedure for NN learning is shown in Fig.4.

### 3.3 NN Generalization and Modification of Z

The trained RBF-NN allows generalization to other test objects. Modification of estimated gradients,

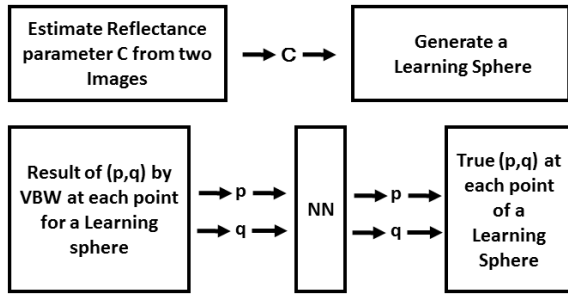


Figure 4: Learning Flow.

$(p, q)$ , is applied to the test object and its depth,  $Z$ , is calculated and updated using the modified gradients,  $(p, q)$ .

In the case of endoscope images, preprocessing is used to remove specularities and to generate a uniform Lambertian image based on (Shimasaki et al., 2013).

Next, the VBW model is applied to the this Lambertian image and the gradients,  $(p, q)$ , are estimated from the obtained  $Z$  distribution.

The estimated gradients,  $(p, q)$ , are input to the NN and modified estimates of  $(p, q)$  are obtained as output from the NN.

Recall that the reflectance parameter,  $C$ , is estimated from  $f(C)$ , based on two images obtained by small movement of endoscope in the  $Z$  direction.

The depth,  $Z$ , is calculated and updated by Eq.(5) using the modified gradients,  $(p, q)$ , and the estimated  $C$ , where Eq.(5) also is the original equation developed in (Iwahori et al., 2010).

$$Z = \sqrt{\frac{CV(-px - qy + f)}{E(p^2 + q^2 + 1)^{\frac{1}{2}}}} \quad (5)$$

Again,  $(p, q) = (\frac{\partial Z}{\partial X}, \frac{\partial Z}{\partial Y})$ ,  $E$  represents image intensity,  $f$  represents the focal length of the lens and  $V = \frac{f^2}{(x^2 + y^2 + f^2)^{\frac{3}{2}}}$ .

A flow diagram of the processing described above is shown in Fig.5.

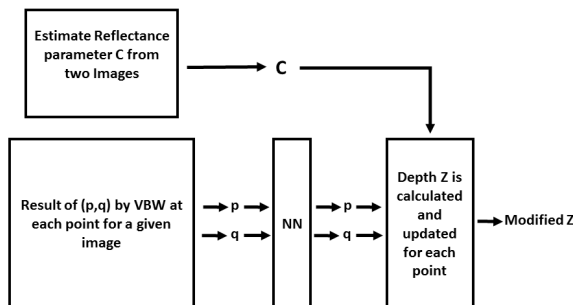


Figure 5: Flow of NN Generalization.

## 4 EXPERIMENTAL RESULTS

### 4.1 NN Learning

A sphere was synthesized with radius 5mm and with center located at  $(0, 0, 15)$ . The focal length of the lens was 10mm. The image size was  $9\text{mm} \times 9\text{mm}$  with pixel size  $256 \times 256$  pixels.

The VBW model was used to recover the shape of this sphere. The resulting gradient estimates,  $(p, q)$ , are shown in Fig.3(b) and (c), respectively.

These estimated gradients,  $(p, q)$ , are used as NN input and the corresponding true gradients,  $(p, q)$ , output from the NN, are shown in Fig.3(d) and (e). Learning was done under the conditions: error goal  $1.0e-1$ , spread constant of the radial basis function 0.00001, and maximum number of learning epochs 500. Learning was complete by about 400 epochs with stable status.

The results of learning is shown in Fig.6.

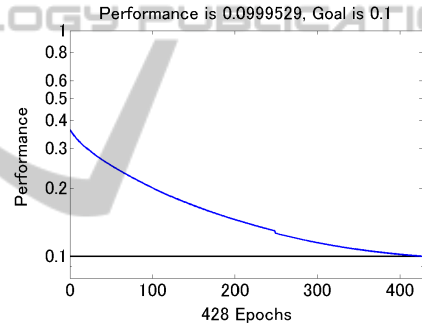


Figure 6: Learning Result.

The reflectance parameter,  $C$ , was estimated as 854 from  $f(C)$ . The difference in depth,  $Z$ , was 0.5 [mm] for the known camera movement.

As shown in Fig.6, NN learning was complete at 428 epochs. The square error goal reached the specified value. Processing time for NN learning was around 30 seconds.

A sphere has a variety of surface gradients and it is used for the NN learning. After a sphere is used for NN learning, not only a sphere object but also other object with another shape including convex or concave surfaces is also available in the generalization process. This is because surface gradient for each point is modified by NN and this modification does not depend on the shape of target object.

### 4.2 Computer Simulation

Computer simulation was performed for a second pair of synthesized images to confirm the performance of

NN generalization. Synthesized cosine curved surfaces were used, one with center located at coordinates  $(0, 0, 12)$  and the other with center at  $(0, 0, 15)$ . Common to both, the reflectance parameter,  $C$ , is 120, the focal length,  $f$ , is 10mm and the waveform cycle is 4mm and the  $\pm$  amplitude is 1mm. Image size is  $5\text{mm} \times 5\text{mm}$  and pixel size is  $256 \times 256$  pixels.

The synthesized image whose center is located at  $(0, 0, 12)$  is shown in Fig.7(a) and the one with center located at  $(0, 0, 15)$  is shown in Fig.7(b).

The reflectance parameter,  $C$ , was estimated according to the proposed method. Using the learned NN, the gradients,  $(p, q)$ , obtained from the VBW model were input and generalized. The gradients,  $(p, q)$ , were modified and the depths,  $Z$ , were updated using Eq.(5).

The graph of the objective function,  $f(C)$ , is shown in Fig.8 and the true depth is shown in Fig.9(a). The estimated  $C$  was 119 (compared to the true value of 120). The estimated  $Z_{diff}$  was 2.9953 (compared to the true value of 3).

The result recovered by VBW for Fig.7(a) is shown in Fig.9(b). The modified values of depth, using the NN and Eq.(5), are shown in Fig.9(c).

Table.1 gives the mean errors in surface gradient and depth estimation. The percentages given in the  $Z$  column represent the error relative to the amplitude of maximum–minimum depth ( $=4\text{mm}$ ) of the cosine synthesized function. In Table 1, the original VBW results have a mean error of around 3.8 degrees for the surface gradient while the proposed approach reduced the mean error to about 0.1 degree. Depth estimation also improved to a mean error of 8.3% from 43.1%. NN generalization improved estimation of shape for an object with different size and shape. It took 9 seconds to recover the shape while it took 61 seconds for NN learning with 428 learning epochs, that is, it took 70 seconds in total.

Computer simulation was performed for a second pair of synthesized images to confirm the performance of NN generalization. Synthesized cosine curved surfaces were used, one with center located at coordinates  $(0, 0, 12)$  and the other with center at  $(0, 0, 15)$ . Common to both, the reflectance parameter,  $C$ , is 120, the focal length,  $f$ , is 10mm and the waveform cycle is 4mm and the  $\pm$  amplitude is 1mm.

Another experiment was performed under the following assumptions. The reflectance factor,  $C$ , is 590,

Table 1: Mean Error.

	$p$	$q$	$Z[\text{mm}]$
VBW	23.04	23.04	0.86 (43.1%)
Proposed	0.32	0.32	0.25 ( 8.3%)

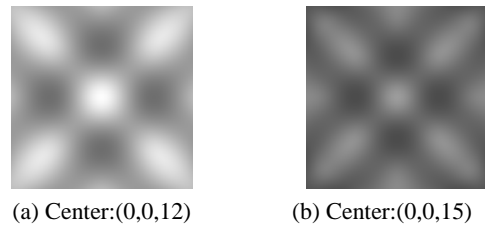


Figure 7: Cosine Model.

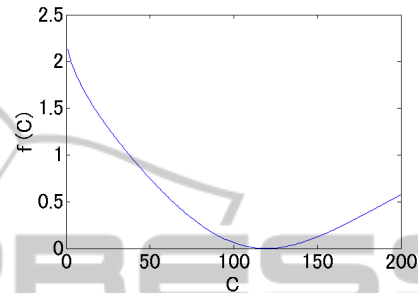


Figure 8: Objective Function  $f(C)$ .

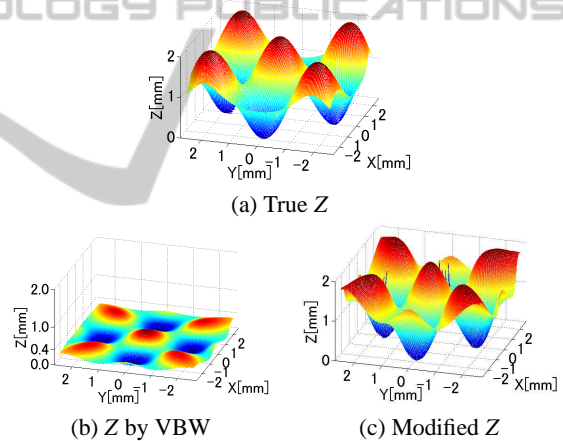


Figure 9: Results.

the focal length,  $f$ , is 10mm and the object is a sphere with radius 5mm. The centers for two positions of the sphere were set at  $(0, 0, 15)$  and  $(0, 0, 17)$  respectively, as shown in Fig.10. The image size was  $9\text{mm} \times 9\text{mm}$  with pixel size  $360 \times 360$  pixels. Here, 4% Gaussian noise (mean 0, variance 0.02, standard deviation 0.14142) is added to each of the two input images. The graph of the objective function,  $f(C)$ , is shown in Fig.11 and the true depth is shown in Fig.12(a). The result recovered by VBW is shown in Fig.12(b). The improved result is shown in Fig.12(c). The mean errors in surface gradient and depth are shown in Table 2. Evaluations for 6% (mean 0, variance 0.03, standard deviation 0.17320) and 10% (mean 0, variance 0.03, standard deviation 0.17320) Gaussian noise included in Table 3, as well.

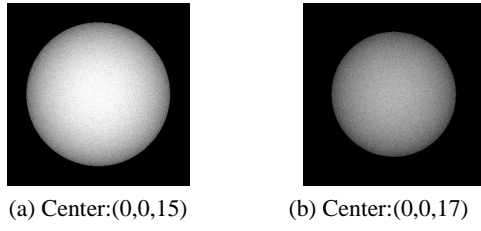


Figure 10: Sphere Images with Gaussian Noise.

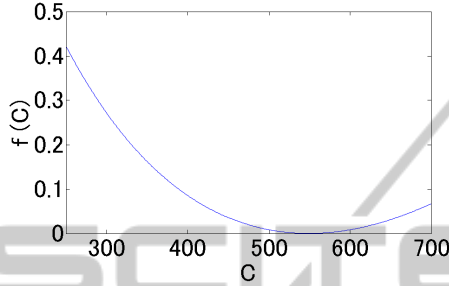
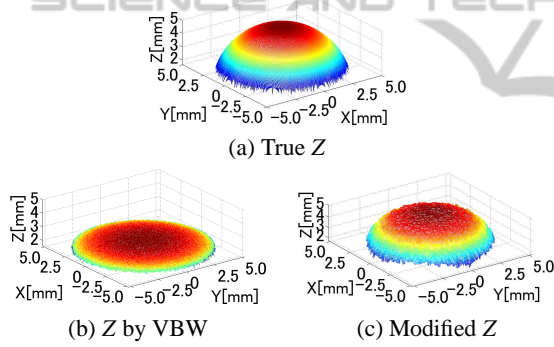

 Figure 11: Objective Function  $f(C)$ .


Figure 12: Results.

Table 2: Mean Error.

	$p$	$q$	$Z$ [mm]
VBW	17.04	17.45	3.36 (67.2%)
Proposed	0.45	0.45	0.36 ( 7.2%)

 Table 3: Mean Error of  $Z$  for Different Gaussian Noise.

	4%	6%	10%
VBW	3.36 (67.2%)	3.25 (65.1%)	2.82 (56.6%)
Proposed	0.36 ( 7.2%)	0.36 ( 7.2%)	0.36 ( 7.3%)

Learning epochs for Gaussian noise 4%, 6% and 10% were 212, 212 and 210. Processing time was around 40 seconds for every case of different Gaussian noises.

The reflectance parameter,  $C$ , estimated from Fig.11, was 591. Improvement in the estimated results is shown in Fig.12(a)(b)(c) and Table 2.

In all three cases, Gaussian noise of 4%, 6% and

10%, the proposed approach reduced the mean error in  $Z$  significantly compared to the original VBW model.

This suggests generalization using the RBF-NN is robust to noise and is applicable to real imaging situations, including endoscopy. Result of VBW model gives less errors with noises but this is based on the result that the recovered shape is relative scale and sensitive to the original intensity of each point according to Gaussian noise, while the proposed approach gives much better shape with the absolute size. Although the error increases a little bit according to Gaussian noise, the approach is still robust and stable result is obtained.

### 4.3 Real Image Experiments

Two endoscope images obtained with camera movement in the  $Z$  direction are used in the experiments.

The reflectance parameter,  $C$ , was estimated and a RBF-NN was learned using a sphere synthesized with the estimated  $C$ . VBW was applied to one of the images which was first converted to a uniform Lambertian image.

Surface gradients,  $(p, q)$ , were modified with the NN then depth,  $Z$ , was calculated and updated at each image point. The focal length,  $f=10\text{mm}$ , the image size  $5\text{mm} \times 5\text{mm}$ , and camera movement,  $\Delta Z=3\text{mm}$ , were assigned to the same known values as those in the computer simulation. The error goal was set to be 0.1.

The two endoscope images are shown in Fig.13(a) and (b). The generated Lambertian images are shown in Fig.13(c) and (d), respectively.

The objective function,  $f(C)$ , is shown in Fig.14.

The result from the VBW model is shown in Fig.15(a) and the modified result is shown in Fig.15(b).

The estimated value of the reflectance parameter,  $C$ , was 1141. The difference in depth,  $Z$ , at the local maximum point was 1 [mm] for the camera movement  $Z_{diff}$  between two images. In Fig.13(c)(d), specularities were removed compared to Fig.13(a)(b). The converted images are gray scale with the appearance of uniform reflectance. Fig.15(b) gives a larger depth range than Fig.15(a). This suggests depth estimation is improved. The size of the polyp was 1cm and the processing time for shape modification was 9 seconds. As it took 117 seconds for NN learning with 540 epochs, a total processing time was 126 seconds.

Although quantitative evaluation is difficult, medical doctors with experience in endoscopy qualitatively evaluated the result to confirm its correctness. Different values of the reflectance parameter,

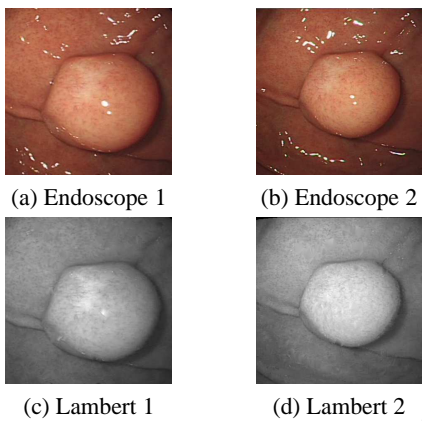


Figure 13: Endoscope Image and Generating Lambert Image.

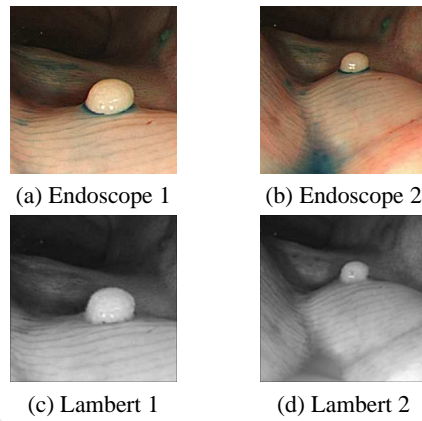


Figure 16: Endoscope Image and Generating Lambert Image.

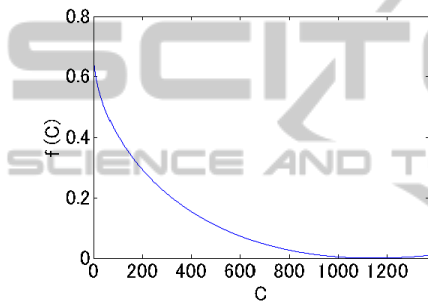


Figure 14: Objective Function  $f(C)$ .

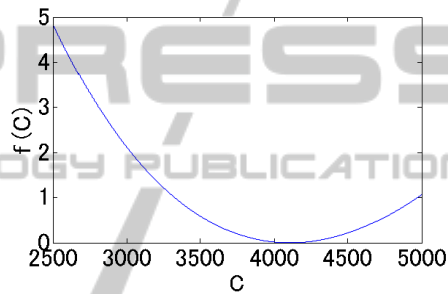


Figure 17: Objective Function  $f(C)$ .

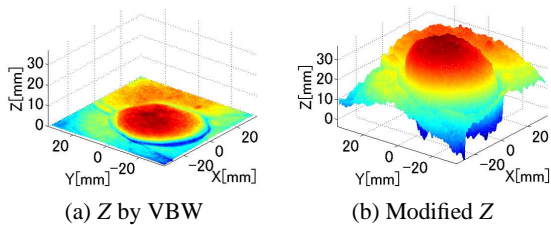


Figure 15: Result for Endoscope Images.

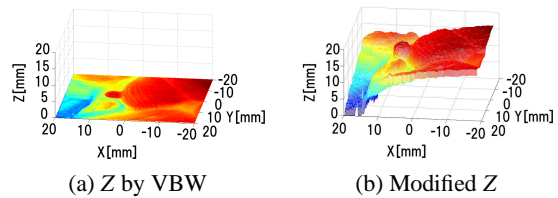


Figure 18: Result for Endoscope Images.

$C$ , were estimated in different experimental environments. The absolute size of a polyp is estimated based on the estimated value of  $C$ . Accurate values of  $C$  lead to accurate estimation of the size of the polyp. The estimated polyp sizes were seen as reasonable by the medical doctor. This qualitatively confirms that the proposed approach is effective in real endoscopy.

Another experiment was done for the endoscope images shown in Fig.16(a)(b). The generated gray scale Lambertian images are shown in Fig.16(c)(d), respectively. Here the focal length is 10mm, image size is 5mm×5mm, pixel size is 256×256 and  $\Delta Z$  was set to be 10mm.

The graph of  $f(C)$  is shown in Fig.17. The VBW result for Fig.16(d) is shown in Fig.18(a), while that for the proposed approach is shown in Fig.18(b).

$C$  was estimated as 4108 from Fig.17. Fig.18(b) shows greater depth amplitude compared to Fig.18(a).

The estimated size of the polyp was about 5mm. This corresponds to the convex and concave shape estimation based on a stain solution. It took 60 seconds for NN learning with 420 epochs and a total processing time was 70 seconds.

4% Gaussian noise was added to a real image and the corresponding results are shown in Fig.19(a). Shape was estimated from the generated Lambertian image, shown in Fig.19(b). The corresponding results are shown in Fig.19(c) and Fig.19(d). Here the focal length is 10mm, image size is 5mm×5mm, pixel size is 256×256 and  $\Delta Z$  was 3mm.

In this paper, it is assumed that movement of the endoscope is constrained to be in the depth,  $Z$ , direction only. Here, it is seen that the result is acceptable

even when camera movement is in another direction, provided rotation is minimal and the overall camera movement is still small.

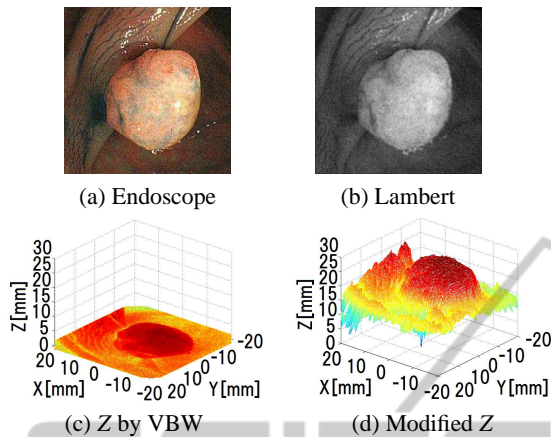


Figure 19: Result with Gaussian Noise.

The reflectance parameter,  $C$ , was estimated as 13244 and Fig.19(b) shows the final estimated shape. Total of processing time was 90 seconds including 80 seconds for NN learning with 480 epochs.

The estimated size of this polyp was about 1cm. Although Gaussian noise was added, shape recovery remained robust.

## 5 CONCLUSION

This paper proposed a new approach to improve the accuracy of absolute size and shape determination of polyps observed in endoscope images.

An RBF-NN was used to modify surface gradient estimation based on training with data from a synthesized sphere. The VBW model was used to estimate a baseline shape. Modification of gradients with the RBF-NN improved the accuracy of that baseline shape estimation. Estimation of the reflectance parameter,  $C$ , was achieved under the assumption that two images are acquired via small camera movement in the depth,  $Z$ , direction. The RBF-NN is non-parametric in that no parametric functional form has been assumed for gradient modification. The approach was evaluated both in computer simulation and with real endoscope images. Results confirm that the approach improves the accuracy of recovered shape to within error ranges that are practical for polyp analysis in endoscopy.

## ACKNOWLEDGEMENT

Iwahori's research is supported by Japan Society for the Promotion of Science (JSPS) Grant-in-Aid for Scientific Research (C) (26330210) and Chubu University Grant. Woodham's research is supported by the Natural Sciences and Engineering Research Council (NSERC). The authors would like to thank Kodai Inaba for his experimental help and the related member for useful discussions in this paper.

## REFERENCES

- Benton, S. H. (1977). The Hamilton- Jacobi Equation: A Global Approach. In *Academic Press, Volume 131*.
- Ding, Y., Iwahori, Y., Nakamura, T., He, L., Woodham, R. J., and Itoh, H. (2010). Shape Recovery of Color Textured Object Using Fast Marching Method via Self-Calibration. In *EUVIP 2010*, pp. 92-96.
- Ding, Y., Iwahori, Y., Nakamura, T., Woodham, R. J., He, L., and Itoh, H. (2009). Self-calibration and Image Rendering Using RBF Neural Network. In *KES 2009, Volume 5712*, pp. 705-712.
- Horn, B. K. P. (1975). Obtaining Shape from Shading Information. In *The Psychology of Computer Vision*, Winston, P. H. (Ed.), Mc Graw- Hill, pp. 115-155. Mc Graw- Hill.
- Iwahori, Y., Iwai, K., Woodham, R. J., Kawanaka, H., Fukui, S., and Kasugai, K. (2010). Extending Fast Marching Method under Point Light Source Illumination and Perspective Projection. In *ICPR2010*, pp. 1650-1653.
- Iwahori, Y., Shibata, K., Kawanaka, H., Funahashi, K., Woodham, R. J., and Adachi, Y. (2014). Shape from SEM Image Using Fast Marching Method and Intensity Modification by Neural Network. In *Recent Advances in Knowledge-based Paradigms and Applications, Advances in Intelligent Systems and Computing 234*, Springer, Chapter 5, pp.73-86.
- Iwahori, Y., Sugie, H., and Ishii, N. (1990). Reconstructing Shape from Shading Images under Point Light Source Illumination. In *ICPR 1990, Vol.1*, pp. 83-87.
- Iwahori, Y., Woodham, R. J., Ozaki, M., Tanaka, H., and Ishii, N. (1997). Neural Network based Photometric Stereo with a Nearby Rotational Moving Light Source. In *IEICE Trans. Info. and Syst., Vol. E80-D, No. 9*, pp. 948-957.
- Kimmel, R. and Sethian, J. A. (2001). Optimal Algorithm for Shape from Shading and Path Planning. In *Journal of Mathematical Imaging and Vision (JMIV) 2001, Vol. 14, No. 3*, pp. 237-244.
- Mourgues, F., Devernay, F., and Coste-Maniere, E. (2001). 3D reconstruction of the operating field for image overlay in 3D-endoscopic surgery. In *Proceedings of the IEEE and ACM International Symposium on Augmented Reality (ISAR)*, pp. 191-192.

- Nakatani, H., Abe, K., Miyakawa, A., and Terakawa, S. (2007). Three-dimensional measurement endoscope system with virtual rulers. In *Journal of Biomedical Optics*, 12(5):051803.
- Neog, D. R., Iwahori, Y., Bhuyan, M. K., Woodham, R. J., and Kasugai, K. (2011). Shape from an Endoscope Image Using Extended Fast Marching Method. In *Proc. of ICAI-11*, pp. 1006-1015.
- Prados, E. and Faugeras, O. (2003). A mathematical and algorithmic study of the Lambertian SFS problem for orthographic and pinhole cameras. In *Technical Report 5005, INRIA 2003*.
- Prados, E. and Faugeras, O. (2005). Shape From Shading: a well-posed problem? In *CVPR 2005*, pp. 870-877.
- Prados, E. and Faugeras, O. D. (2004). Unifying Approaches and Removing Unrealistic Assumptions in Shape from Shading: Mathematics Can Help. In *ECCV04*.
- Sethian, J. A. (1996). A Fast Marching Level Set Method for Monotonically Advancing Fronts. In *Proceedings of the National Academy of Sciences of the United States of America (PNAS U.S.)*, Vol. 93, No. 4, pp. 1591-1593.
- Shimasaki, Y., Iwahori, Y., Neog, D. R., Woodham, R. J., and Bhuyan, M. K. (2013). Generating Lambertian Image with Uniform Reflectance for Endoscope Image. In *IWAIT2013, 1C-2 (Computer Vision 1)*, pp. 60-65.
- Tatematsu, K., Iwahori, Y., Nakamura, T., Fukui, S., Woodham, R. J., and Kasugai, K. (2013). Shape from Endoscope Image based on Photometric and Geometric Constraints. In *KES 2013, Procedia Computer Science, Elsevier, Vol.22*, pp. 1285-1293.
- Thormaehlen, T., Broszio, H., and Meier, P. N. (2001). Three-Dimensional Endoscopy. In *Falk Symposium*, pp. 199-212.
- Vogel, O., Breuß, M., and Weickert, J. (2007). A Direct Numerical Approach to Perspective Shape-from-Shading. In *Vision Modeling and Visualization (VMV) 2007*, pp. 91-100.
- Yuen, S. Y., Tsui, Y. Y., and Chow, C. K. (2007). A fast marching formulation of perspective shape from shading under frontal illumination. In *Pattern Recognition Letters*, Vol. 28, No.7, pp. 806-824.